Chemical Papers (2022) 76:2041–2050
https://doi.org/10.1007/s11696-021-01981-5

ORIGINAL PAPER

Anthracene modified graphene for C_{60}/C_{70} fullerenes capture and construction of energy storage materials

Agata Fedorczyk[1] · Agnieszka Krogul-Sobczak[1] · Piotr Piotrowski[1]

Received: 29 June 2021 / Accepted: 10 November 2021 / Published online: 28 December 2021

Abstract

Graphene functionalized with dianthracene malonate was synthesized and used subsequently for construction of covalently bound graphene-fullerene hybrid nanomaterials. For this purpose, novel approach of Diels–Alder reaction of C_{60}/C_{70} fullerene cores with anthracene moieties previously introduced onto graphene surface was successfully employed. Structure and composition of obtained graphene and its derivatives were characterized using scanning electron microscopy (SEM), X-ray photoelectron spectroscopy (XPS) and FT-IR spectroscopy. Obtained results revealed that both C_{60} and C_{70} fullerenes were found to be capable of formation desired Diels–Alder adducts, yielding products of different morphology. Capacitive properties of the synthesized energy storage nanomaterials were determined by means of cyclic voltammetry (CV) and galvanostatic charge/discharge (GCD) measurements, revealing that functionalization of graphene with C_{60} moieties enhances its energy storage properties.

Keyword Graphene-fullerene energy storage capacitor

Introduction

Nowadays we can observe increasing demand for high power, capacitance, light weight and long-life energy storage materials. For this purpose, supercapacitors are most promising candidates (Poonam et al. 2019; González et al. 2016) because of their high power density, long cycle life, fast charge/discharge rates and low maintenance cost. Carbon-based materials are often the choice for the capacitor electrodes (Najib et al. 2019; Dubey et al. 2019). One of the carbon nanomaterials with a 2D structure, high and accessible surface area, exceptional intrinsic electrical conductivity, high temperature stability is currently widely studied graphene (Ke et al. 2016; Lemine et al. 2018; Li et al. 2019a, b). Despite advantageous properties of its pristine form, there some drawbacks of unmodified graphene. This include, among other its zero band-gap and difficulty in formation of stable dispersions in organic solvents. However, tailored functionalization of graphene can lead to improvement of its properties, along with gaining new features coming from introduced functionalities.

When considering the functionalization of graphene there are two main approaches to achieve this goal described in the literature. First strategy is based on various non-covalent methods that allow to modify graphene surface (Georgakilas et al. 2016; Zhao et al. 2021). For this purpose, molecules with planar conjugated π-systems are usually chosen due to their van der Waals, electrostatic or π–π stacking interactions with graphene surface. One of the main advantages of this type of graphene derivatives is their non-disrupted, extended π-conjugation of carbon atoms on the graphene surface. Resulting graphene retains its remarkable properties, showing less defective structure and higher conductivity when comparing to less conjugated graphene (Su et al. 2013; Jin et al. 2017). These nanomaterials have found applications in the fields of drug delivery (Liu et al. 2013), energy materials (Cai et al. 2019), solar cells (Mahmoudi et al. 2018), water splitting (Li et al. 2019a, b), biosensing (Pumera 2011; Peña-Bahamonde et al. 2018), environmental (Perreault et al. 2015), catalytic (Haag et al. 2014) and biomedical technologies (Shareena et al. 2018).

On the other hand, numerous synthetic procedures for covalent modification of graphene, which provide more stable arrays comparing to those based on secondary interactions,

✉ Piotr Piotrowski
ppiotrowski@chem.uw.edu.pl

[1] Department of Chemistry, University of Warsaw, Pasteura 1, 02-093 Warsaw, Poland

were reported (Bottari et al. 2017). Those reactions can be divided into two main groups: formation of covalent bond by reactions with the oxygen groups present on the graphene oxide surface or formation of covalent bond by addition to the graphene C=C double bond. The second type of reactions involves mainly organic radicals and dienophiles as reagents, and include cycloaddition reactions, which have been successfully employed for functionalization of graphene surface. One of the examples of such approach is the so-called Bingel reaction, well known from the chemistry of fullerenes, but also already employed in functionalization of carbon nanotubes and graphene (Naebe et al. 2015; Jin et al. 2016).

Similarly to graphene, fullerenes due to their unique physical and chemical properties, remarkable electron-accepting features and solubility in organic solvents, along with various methods of their functionalization are also interesting platform for construction of energy storage materials (Wang et al. 2017; Khan et al. 2019; Bairi et al. 2019). It would be very interesting to create novel hybrid nanomaterial composed of graphene and fullerene, as it is expected that binding of fullerenes to graphene surface should not only increase the capacity of resulting hybrid nanomaterial (Ma et al. 2015; Cerón et al. 2019) but also provide adequate stability and prevent restacking of graphene sheets (Wang et al. 2009). Reports on not only performance comparison for capacitors based on C_{60} or C_{70} fullerenes (Tran et al. 2009) but also on energy storage application of C_{70} and its derivatives are scarce (Bairi et al. 2016).

In this contribution, we report herein, synthesis of graphene functionalized with C_{60} and C_{70} fullerenes by novel approach based on Diels–Alder reaction of fullerene core with anthracene derivative. Necessary anthracene moieties were covalently bound onto graphene surface via Bingel reaction using corresponding dianthracene malonate, ensuring high stability of obtained nanomaterial. Functionalized graphene showed fullerene binding capability due to Diels–Alder reaction of anthracene moieties with fullerene cores, both C_{60} and C_{70}. Obtained graphene-fullerene hybrids were studied using electrochemical methods, and impact of the fullerene core type on energy storage properties was determined. Results obtained using cyclic voltammetry (CV) and galvanostatic charge/discharge (GCD) measurements showed that presence fullerene core influences the energy storage ability and introduction of appropriate fullerene molecules can improve the final capacitance of synthesized nanomaterials.

Experimental

Chemicals

9-Anthracenemethanol, ethyl acetate, *n*-hexane, 1,2-dichlorobenzene (ODCB), malonyl chloride, potassium hydroxide, toluene and Nafion™ (5wt.%) were bought from Sigma-Aldrich. Carbon tetrabromide, 1,8-diazabicyclo(5.4.0) undec-7-ene (DBU), *N*-methylpyrrolidone and silica gel (0.060–0.2 mm, 70–230 mesh) were purchased from Alfa Aesar. Acetone, dichloromethane, ethanol, magnesium sulfate, methylene blue, trimethylamine and potassium hydroxide were bought from POCh (Poland). C_{60} and C_{70} fullerene were purchased from Nano-C. Toluene was dried and purified before use by refluxing with sodium and benzophenone under argon atmosphere, other solvents were analytical grade reagents and were used as received.

Characterization methods and instrumentation

Mass spectra were recorded using Micromass LCT ESI-TOF mass spectrometer equipped with an orthogonal electrospray ionization source. ^{1}H and ^{13}C nuclear magnetic resonance (NMR) spectra were recorded on Varian Unity Plus 500 MHz spectrometer using $CDCl_3$ as a solvent. The infrared experiments were carried out using the Shimadzu FTIR-8400S. X-ray Photoelectron Spectroscopy (XPS) measurements were carried out using a VG ESCALAB 210 electron spectrometer equipped with an Al Kα source (1486.6 eV). XPS data were calibrated using the binding energy of C1s = 284.6 eV as the internal standard. UV–Vis spectra were recorded using Varian Cary 50 UV–Vis spectrophotometer. Scanning electron microscopy analysis was performed using Merlin SEM (Zeiss). Electrochemical experiments were carried out using the potentiostat PGSTAT 30 N (Metrohm, Autolab, The Netherlands). All experiments were performed at room temperature in 3 M KOH as supporting electrolyte, in a three-electrode cell with a silver/silver chloride (Ag/AgCl) as the reference electrode and platinum foil counter electrode. The working electrode was a gold disk of the surface area of 0.2 cm^2.

Synthesis of bis(anthracen-9-ylmethyl) malonate (Fig. 1)

9-Anthracenemethanol (3 g, 14.4 mmol) was added to a stirred solution of triethylamine (1.46 g, 14.4 mmol) in anhydrous dichloromethane (60 ml) at room temperature and under argon

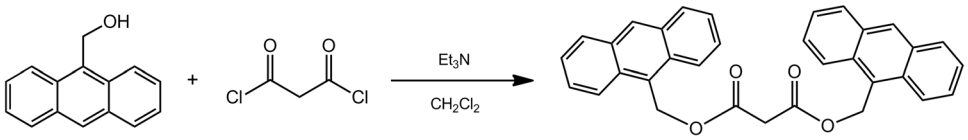

Fig. 1 Synthesis of bis(anthracen-9-ylmethyl) malonate (**BAM**)

atmosphere. The resulting solution was cooled to 0 °C using an ice bath. Afterward, malonyl chloride (1.02 g, 7.2 mmol) diluted with 5 ml of anhydrous methylene chloride was added dropwise in the period of 45 min. Then mixture was allowed to warm to room temperature and was stirred for additional 3 h. Then it was diluted with ethyl acetate, washed twice with water and dried using anhydrous magnesium sulfate. Then, the solvent was removed at reduced pressure. Purification of the product was accomplished by the means of flash column chromatography (1:2.5 ethyl acetate: n-hexane) to give desired product as yellow solid.

Yield: 89%, Mp 191 °C, lit. 178–182 °C (Herranz et al. 2004), the mass spectrum (ESI–MS) showed a $[M+Na]^+$ peak at 507.7 (Figure S1, Supplementary Information, SI); IR (KBr disk) $\nu_{max}(cm^{-1})$ 3085.27, 3036.83, 3001.65, 2960.30, 2916.11, 2848.30, 2359.83, 1747.57, 1722.21, 1383.12, 1352.70, 1330.53, 1171.30, 982.33, 883.91, 735.78, 728.82 (Figure S2, SI); NMR (literature data can be found in Herranz et al. 2004) δ^1H 500 MHz; $CDCl_3$; TMS) 8.47 (s, 2H), 8.18–8.20 (q, 4H), 7.97–7.99 (q, 4H), 7.43–7.46 (m, 8H), 6.12 (s, 2H), 3.40 (s, 2H) ppm (Figure S3, SI); $\delta^{13}C$ (125 MHz; $CDCl_3$) 166.76, 131.31, 131.07, 129.44, 129.08, 126.77, 125.13, 123.76, 59.97, 41.47 ppm (Figure S4, SI); UV–Vis $\lambda_{max} = 334.4$, 350.5, 368.5, 387.6 nm (Figure S5, SI).

Preparation of graphene

Graphene was prepared by exfoliation of graphite in liquid phase using ultrasonic treatment (Quintana et al. 2010; Georgakilas et al. 2010). Briefly, 40 mg of graphite was ultrasonically dispersed in 300 ml of *N*-methylpyrrolidone (NMP) and sonicated for 30 min. Obtained dispersion was centrifuged carefully for 20 min at 1000 rpm, resulting solid was washed with methanol.

Functionalization of graphene by the Bingel reaction

To a well stirred dispersion of graphene (20 mg) in *o*-dichlorbenzene (50 ml), bis(anthracen-9-ylmethyl) malonate (49 mg, 0.1 mmol) and tetrabromomethane (33 mg, 01.mmol) were added. Afterward, solution of DBU (75 µl, 0.5 mmol) in *o*-dichlorbenzene (5 ml) was added slowly under argon atmosphere. Resulting reaction mixture was stirred for 24 h at room temperature. Then it was centrifuged at 1000 rpm for 30 min, and washed twice with toluene and *n*-pentane. Obtained anthracene functionalized graphene (**GA**) was dried under vacuum and examined by SEM, FT-IR, XPS and CV, and used in further Diels–Alder reaction with selected fullerenes.

Diels–Alder reaction of fullerenes and anthracene functionalized graphene

Fullerene-graphene hybrid nanomaterials (**GAF6/GAF7**) were prepared via Diels–Alder reaction using modified method reported by our group previously for anthracene functionalized gold electrodes (Piotrowski et al. 2016). For this purpose, 10 mg of anthracene functionalized graphene was dispersed in $1 \cdot 10^{-3}$ M toluene solution of corresponding fullerene (12 ml). After stirring for 72 h, obtained mixture was centrifuged at 1000 rpm for 30 min. Resulting solids were washed twice with toluene to remove unbound fullerenes and dried under vacuum at 40 °C. Obtained samples of graphene/fullerene composites were subsequently analyzed by SEM, FT-IR, XPS and CV techniques (Figs. 2, 3).

Results and discussion

Scanning electron microscopy (SEM)

Morphology of obtained nanostructures, i.e., pristine graphene and its **GA** and **GAF** derivatives was analyzed using scanning electron microscopy (Fig. 4). Graphene obtained by exfoliation of graphite in NMP (Fig. 4A) showed 3D structure build from bent single graphene sheets and flakes. After functionalization of graphene with bis-anthracene malonate, we don't observe any visible change in the structure of this nanomaterial (Fig. 4B). No significant

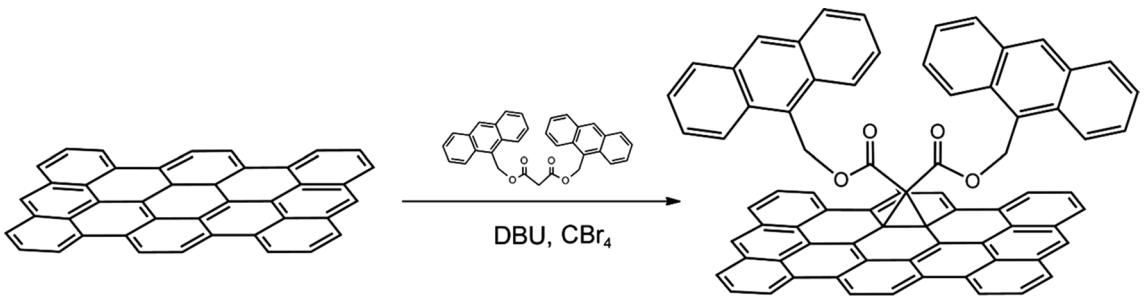

Fig. 2 Synthesis scheme for graphene functionalization with bis-anthracene malonate

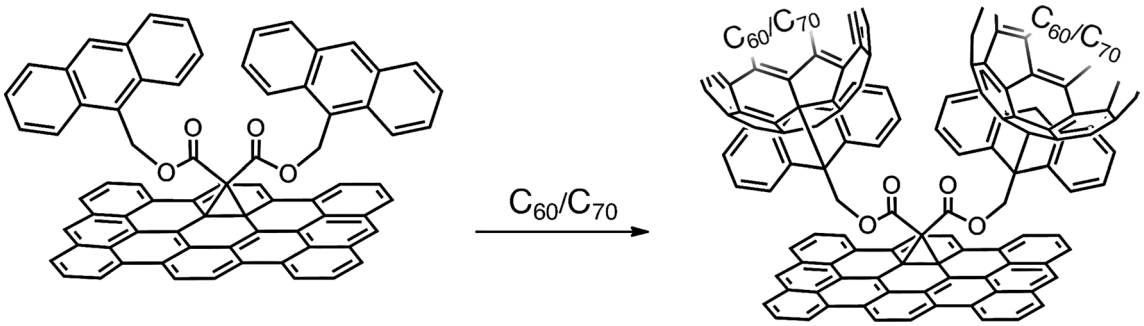

Fig. 3 Scheme for functionalization of anthracene covered graphene **GA** with C_{60} and C_{70} fullerenes via Diels–Alder reaction

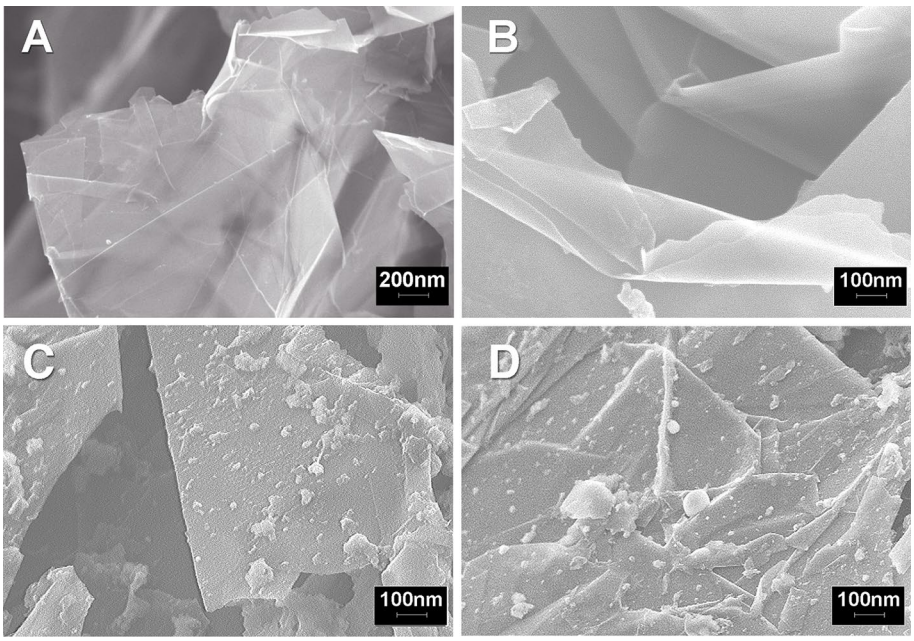

Fig. 4 SEM images of pristine graphene (**a**), graphene covered with anthracene **GA** (**b**), graphene functionalized with C_{60} (**GAF6**) (**c**) and C_{70} (**GAF7**) (**d**) via Diels–Alder reaction

restacking of single graphene sheets can be seen in SEM image, along with any other visible changes when comparing to unmodified graphene. After Diels–Alder reaction of **GA** with C_{60} (Fig. 4C) or C_{70} (Fig. 4D), we can observe presence of granular aggregates on the graphene surface in both samples. When comparing fullerene modified graphenes: **GAF6** and **GAF7**, we can observe that graphene layers modified with C_{70} fullerene (**GAF7**) show higher tendency to restacking. There is also a noticeable difference in the size of observed fullerene aggregates, as C_{70} adducts with **GA** show visibly bigger particle size when comparing to C_{60} analog. To confirm that observation we have performed particle size calculations using ImageJ software (Abramoff et al. 2004) and estimated average diameter of fullerene aggregates on surface of GAF6 and GAF7, which was found to be approximately 24 nm and 34 nm, respectively.

X-ray photoelectron spectroscopy (XPS)

For the investigation of the graphene-based nanomaterials, C1s region of the X-ray photoelectron spectra can give the biggest insight into characterization of obtained composite materials. Deconvoluted C1s core level spectrum of pristine graphene (Fig. 5A) showed presence of two signals centered at 284.6 and 285.5 eV. This peaks are attributed to graphene carbon atoms with sp^2 (at 87% abundance) and sp^3 hybridization (13%at), respectively (Kabir et al. 2019; Lesiak et al. 2018), which indicates low content of defects on graphene surface.

Functionalization of the graphene with anthracene moieties ensue visible changes in the XPS results (Fig. 5B). The spectrum of **GA** in the C1s region was fitted with good correlation into four signals. Main peak observed

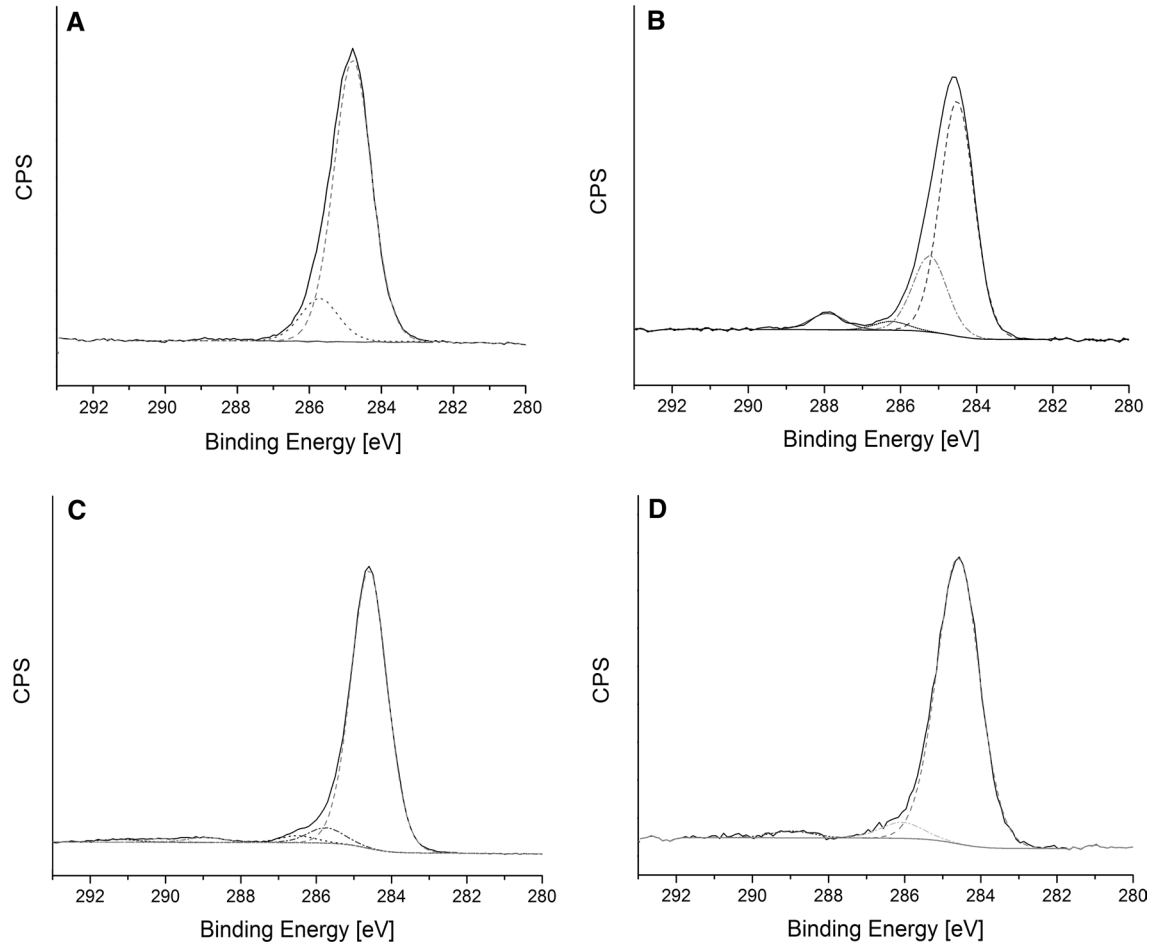

Fig. 5 XPS C1s spectra of pristine graphene (**A**), graphene functionalized with anthracene malonate (**B**), graphene covered with anthracene after Diels–Alder reaction with C_{60} (**C**) and C_{70} (**D**)

at 284.6 eV is attributed to sp^2 carbons coming from both graphene and introduced anthracene malonate (70%at). Raise of the higher binding energy peaks intensity is caused by increased amount of carbon atoms with sp^3 hybridization and was expected after successful addition of anthracene malonate to double bonds of graphene surface. The second biggest peak with 22% abundance is centered at 285.4 eV and is attributed to C–C carbon atoms (Yulaev et al. 2016). The other two peaks are observed due to presence of C–O ester (3%at) and C=O carbonyl (5%at) carbon atoms and where observed at 286.3 and 288.0 eV, respectively (Zuo et al. 2013).

Self–assembly of C_{60} fullerene on the surface of anthracene functionalized graphene via Diels–Alder reaction had also impact on the C1s region of XPS spectrum (Fig. 5C). Deconvolution of registered signal revealed six components centered at 284.6, 285.6, 286.5, 288.9, 290.1 and 291.3 eV, arising from of all expected forms of carbon: C=C, C–C, C–O and C=O, along with two C_{60} fullerene π–π satellite peaks (Leiro et al. 2003; Nakao et al. 1997). Intensity of the lowest energy component (89%at), attributed to sp^2 carbon, was higher when compared to the anthracene modified graphene. This was observed due to deposition of high amount of C_{60} fullerene by Diels–Alder reaction and then secondary growth of aggregates on covalently bound seeds. XPS atomic percent values of other carbon atoms were calculated to be: 5%at (C–C), 2%at (C–O) and 2%at (C=O), and remaining π–π* shake-up features were associated with 2%at. Those results confirm successful formation of fullerene-graphene hybrid nanomaterial (**GAF6**), obtained using Diels–Alder reaction, indicating also that most of fullerenes were physisorbed on the graphene substrate due to formation of aggregates on previously covalently bound C_{60} molecules.

Similarly, XPS spectrum registered for **GAF7** showed noticeable changes in C1s region (Fig. 5D), when comparing to **GA**. C1s region of registered XPS spectrum was fitted with three signals, which can be attributed to C=C/C–C, C–O, C=O, and were observed at correspondingly 284.6, 286.0 and 288.8 eV (Sohmen et al. 1992). The most important difference when comparing foregoing data to the spectra

obtained for **GAF6** sample, is the higher content of the sp^2 carbon atoms. This result is in good agreement with the observations made for SEM images, where the **GAF7** sample showed presence of visibly larger fullerene aggregates.

FT-IR spectroscopy

Formation of graphene-fullerene nanocomposites was also confirmed by means of FT-IR spectroscopy (Fig. 6). When comparing the spectra of pristine graphene (**G**) and its anthracene derivative (**GA**), both share the two signals located at around 820 and 1110 cm^{-1} (Leiro et al. 2003; Güler et al. 2013), frequently reported for grapehenous materials. However, IR spectrum of anhtracene modified graphene indicates serious changes in the composition showing numerous additional bands. Strong signal observed at 1704 cm^{-1}, which is attributed to C=O stretching vibrations indicates introduction of carbonyl groups, coming from malonate adduct. Presence of ester functional groups is also confirmed by C–O stretching bands at 1073 and 1263 cm^{-1}. Aromatic C=C stretching observed at 1563 and 1656 cm^{-1}, along with aromatic C–H stretch at 2966 cm^{-1}, can be assigned to anthracene moieties from introduced malonate, revealing successful functionalization of graphene surface.

FT-IR spectrum after addition of C_{60} fullerene via Diels–Alder reaction retains most characteristic signals observed for graphene and its newly introduced anthracene malonate functional groups. At the same time, signals characteristic for C_{60} molecule were registered at 1422, 564 and 525 cm^{-1} (Bethune et al. 1991), allowing to conclude that anthracene modified graphene reacts with fullerene yielding **GAF6**.

Similarly, addition of C_{70} to anthracene modified graphene also results in presence of additional signals in registered spectrum. Typical C_{70} related bands were registered in **GAF7** sample at 1437, 1130 and 537 cm^{-1} (Bethune et al. 1991), indicating that C_{70} also form Diels–Alder adducts with graphene covered with antrhracene malonate.

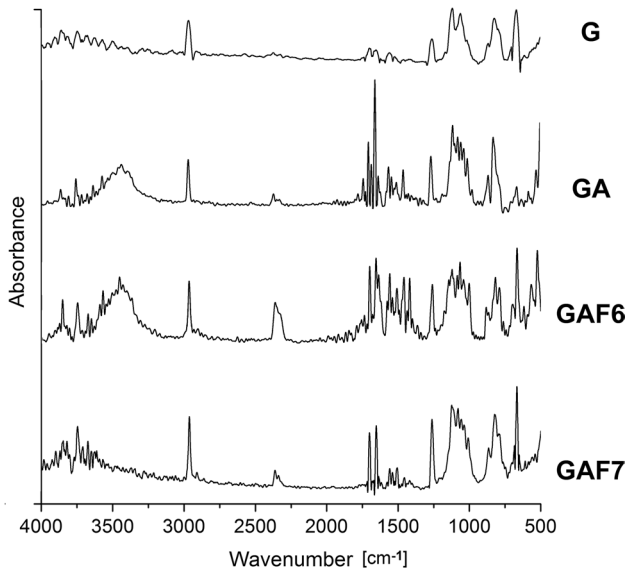

Fig. 6 FT-IR spectra of pristine graphene (**G**), anthracene functionalized graphene (**GA**), Diels–Alder adduct of antracene with fullerene C_{60} (**GAF6**) and C_{70} (**GAF7**) registered in KBr disk

Electrochemical measurements

In order to investigate the capacitive properties of the synthesized nanomaterials, 3 mg of each sample was mixed with 300 µl of ethyl alcohol and 25 µl of Nafion™ solution and left overnight on a magnetic stirrer in order to obtain stable suspension. Prepared samples were applied on the working electrode by dropping a known volume of suspension until the gold surface was completely covered. Such modified electrodes were ready to use in electrochemical experiment after complete evaporation of the solvent. All measurement were conducted in 3 M KOH. Cyclic voltammograms of the synthesized materials in potential range from 0.2 to 1.1 V with a scan rate of 20 mV s^{-1} are shown in Fig. 7. The CV curves for all samples show a quasi-rectangular shape, indicative of the electrochemical double-layer capacitive characteristics.

The specific capacitance (C_s) of electrode materials can be determined from the slope of the linear charge–discharge graph (Fig. 8) according to the equation $C_s = I/(m(dV/dt))$, where I is the applied constant current, dV/dt is the slope of the linear portion of the charge curve, and m is the mass of the materials deposited on the working electrode. The

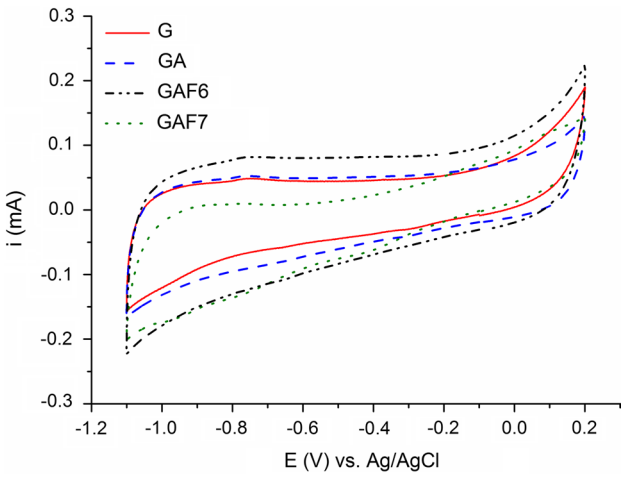

Fig. 7 Comparison of cyclic voltammograms of pristine graphene (**G**), graphene functionalized with anthracene malonate (**GA**), graphene covered with anthracene after Diels–Alder reaction with C_{60} (**GAF6**) and C_{70} (**GAF7**) in 3 M KOH with a scan rate of 20 mV s^{-1}

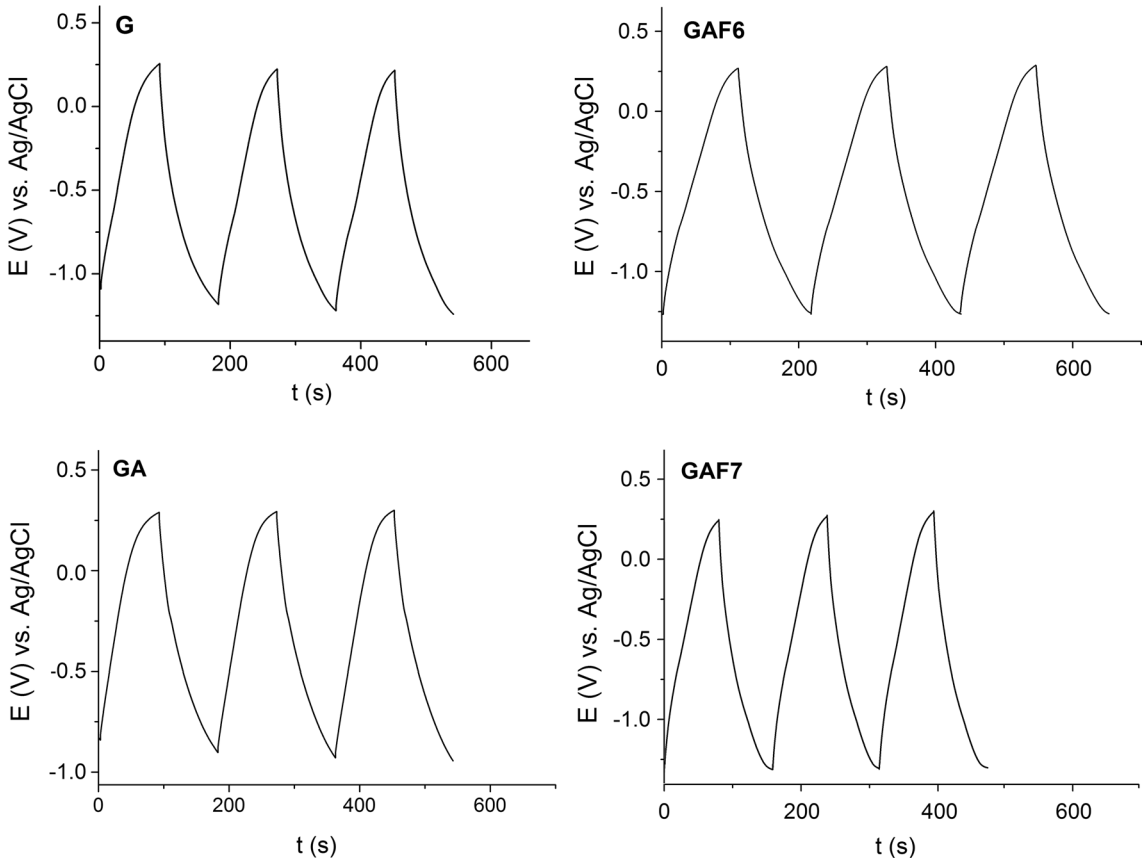

Fig. 8 Galvanostatic charge/discharge curves at the current density of 1 A g^{-1} in 3 M KOH conducted in potential range from 0.2 to 1.2 V for pristine graphene (**G**), graphene functionalized with anthracene malonate (**GA**), graphene covered with anthracene after Diels–Alder reaction with C_{60} (**GAF6**) and C_{70} (**GAF7**)

Table 1 Specific capacitance of obtained electrode materials

Sample	Specific capacitance [F/g]
G	55.0
GA	54.6
GAF6	65.5
GAF7	45.4

calculated specific capacitances of the graphene/fullerene composites were shown in Table 1.

Results indicate that functionalization of graphene with anthracene malonate does not affect the capacitive properties of this material; the values of specific capacitances **G** and **GA** samples are almost the same (55.0 F g^{-1} and 54.6 F g^{-1}, respectively). Among all samples, C_{60} covered graphene (**GAF6**) shows the highest value of specific capacitance (65.5 F g^{-1}). Since the capacitive properties of electrode material are closely related to this part of material which is in direct contact with electrolyte solution, the decreased capacitance for **GAF7** composite (45,4 F g^{-1}) is in quite good agreement with the SEM images where the **GAF7** sample showed presence of visibly larger fullerene aggregates compared to **GAF6**, resulting in lower active surface area. To support this observation, we have determined specific surface area of both nanomaterials using methylene blue method (Chen et al. 2020; Rubino et al. 1999). Results obtained for **GAF6** and **GAF7** are in good agreement with SEM images, as specific surface areas were calculated to be approximately 810 m^2/g and 540 m^2/g, respectively.

The performance and stability of our best energy storage material **GAF6** were studied using GCD measurements for the time of 12 h of continuous charging and discharging (Fig. 9). The first GCD curves reveal highly linear and symmetrical shape, but slow loss of this symmetry and tendency of capacitance drop during cycling is observed. As seen in the capacitance versus number of cycle plots, the electrode retained around 60% of its capacitance after 200 cycles.

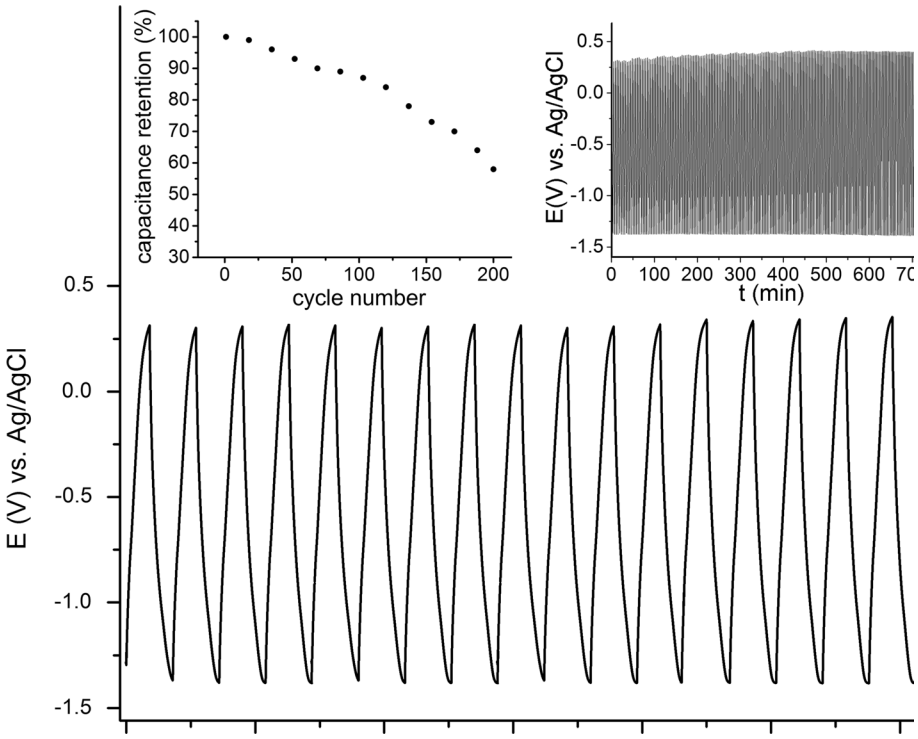

Fig. 9 Potential versus time plot for the first seventeen cycles at the current density of 1 A g^{-1} in 3 M KOH. Inset figures show capacitance retention (left) and GCD curves for 12 h experiment (right)

Conclusions

Graphene functionalized covalently with bis-anthracene malonate using modified Bingel reaction was synthesized and characterized. Facile functionalization method allows to obtain desired graphene/fullerene composites. Reported novel nanomaterial is capable for binding fullerenes via Diels–Alder reaction of introduced anthracene molecules with both C_{60} and C_{70} cores.

Obtained graphene/fullerene composites were successfully employed as energy storage materials. Electrochemical measurements revealed enhanced properties of C_{60} covered graphene (**GAF6**) when comparing to pristine graphene, its anthracene derivative and corresponding C_{70} analog, showing nearly 20% increase in specific capacitance value in comparison to starting material. This can be attributed to high specific surface area of C_{60} fullerene functionalized graphene and fact that C_{60} molecules surface serve as spacers that prevent graphene sheets from restacking.

Presented approach can be further developed, leading to formation advanced hybrid materials consisting of graphene and fullerenes or their derivatives. It can be applied in materials engineering not only for construction of energy storage devices but many other fullerene-graphene composites, where simple synthesis method and resulting covalent binding of fullerene are of great importance.

Supplementary Information The online version contains supplementary material available at https://doi.org/10.1007/s11696-021-01981-5.

Acknowledgements We gratefully acknowledge the financial support from the Polish National Science Center Project no: UMO-2016/21/D/ST5/02874.

Funding Narodowe centrum nauki,UMO-2016/21/D/ST5/02874,Piotr Piotrowski.

References

Abramoff MD, Magalhaes PJ, Ram SJ (2004) Image Processing with ImageJ. Biophotonics Int 11:36–42

Bairi P, Shrestha RG, Hill JP, Nishimura T, Ariga K, Shrestha LK (2016) Mesoporous graphitic carbon microtubes derived from fullerene C70 tubes as a high performance electrode material for advanced supercapacitors. J Mater Chem A 4:13899–13906. https://doi.org/10.1039/C6TA04970B

Bairi P, Maji S, Hill JP, Kim JH, Ariga K, Shrestha LK (2019) Mesoporous carbon cubes derived from fullerene crystals as a high rate performance electrode material for supercapacitors. J

Mater Chem A 7:12654–12660. https://doi.org/10.1039/C9TA00520J

Bethune DS, Meijer G, Tang WC, Rosen HJ, Golden WG, Seki H, Brown CA, de Vries MS (1991) Vibrational Raman and infrared spectra of chromatographically separated C_{60} and C_{70} fullerene clusters. Chem Phys Lett 179:181–186. https://doi.org/10.1016/0009-2614(91)90312-W

Bottari G, Herranz MA, Wibmer L, Volland M, Rodriguez-Perez L, Guldi DM, Hirsch A, Martin N, D'Souza F, Torres T (2017) Chemical functionalization and characterizationof graphene-based materials. Chem Soc Rev 46:4464–4500. https://doi.org/10.1039/C7CS00229G

Cai L, Yu G (2019) Recent advances in growth and modification of graphene-based energy materials: from chemical vapor deposition to reduction of graphene oxide. Small Methods 3:1900071. https://doi.org/10.1002/smtd.201900071

Cerón MR, Zhan C, Campbell PG, Freyman MC, Santoyo C, Echegoyen L, Wood BC, Biener J, Pham TA, Biener MM (2019) Integration of fullerenes as electron acceptors in 3D graphene networks: enhanced charge transfer and stability through molecular design. ACS Appl Mater Interfaces 11:28818–288822. https://doi.org/10.1021/acsami.9b06681

Chen L, Batchelor-McAuley C, Rasche B, Johnston C, Hindle N, Compton RG (2020) Surface area measurements of graphene and graphene oxide samples: Dopamine adsorption as a complement or alternative to methylene blue? Applied Materials Today 18:100506. https://doi.org/10.1016/j.apmt.2019.100506

Dubey R, Guruviah V (2019) Review of carbon-based electrode materials for supercapacitor energy storage. Ionics 25:1419–1445. https://doi.org/10.1007/s11581-019-02874-0

Georgakilas V, Bourlinos AB, Zboril R, Steriotis TA, Dallas P, Stubos AK, Trapalis C (2010) Organic functionalisation of graphenes. Chem Commun 46:1766–1768. https://doi.org/10.1039/B922081J

Georgakilas V, Tiwari JN, Kemp KC, Perman JA, Bourlinos AB, Kim KS, Zboril R (2016) Noncovalent functionalization of graphene and graphene oxide for energy materials, biosensing, catalytic, and biomedical applications. Chem Rev 116:5464–5519. https://doi.org/10.1021/acs.chemrev.5b00620

González A, Goikolea E, Barrena JA, Mysyk R (2016) Review on supercapacitors: technologies and materials. Renew Sustain Energy Rev 58:1189–1206. https://doi.org/10.1016/j.rser.2015.12.249

Güler Ö, Güler SH, Selen V, Albayrak MG, Evin E (2013) Production of graphene layer by liquid-phase exfoliation with low sonication power and sonication time from synthesized expanded graphite. Fullerenes Nanotubes Carbon Nanostruct 24:123–127. https://doi.org/10.1080/1536383X.2015.1114472

Haag D, Kung HH (2014) Metal free graphene based catalysts: a review. Top Catal 57:762–773. https://doi.org/10.1007/s11244-013-0233-9

Herranz MÁ, Echegoyen L (2004) Tandem addition reactions of dialkoxyanthracenes with C60. Thermal vs. electrochemical stability of Diels-Alder adducts. New J Chem 28:513–518

Jin L, Liu T (2016) Chemical vapor deposition monolayer graphenefunctionalization by the Bingel reaction. J Macromolecular Sci Part A 53:433–437. https://doi.org/10.1080/10601325.2016.1176444

Jin E, Asada M, Xu Q, Dalapati S, Addicoat MA, Brady MA, Xu H, Nakamura T, Heine T, Chen Q, Jiang D (2017) Two-dimensional sp^2 carbon–conjugated covalent organic frameworks. Science 357:673–676. https://doi.org/10.1126/science.aan0202

Kabir H, Zhu H, May J, Hamal K, Kan Y, Williams T, Echeverria E, McIlroy DN, Estrada D, Davis PH, Pandhi T, Yocham K, Higginbotham K, Clearfield A, Cheng IF (2019) The sp2-sp3 carbon hybridization content of nanocrystalline graphite from pyrolyzed vegetable oil, comparison of electrochemistry and physical properties with other carbon forms and allotropes. Carbon 144:831–840. https://doi.org/10.1016/j.carbon.2018.12.058

Ke Q, Wang J (2016) Graphene-based materials for supercapacitor electrodes—a review. J Matriomics 2:37–54. https://doi.org/10.1016/j.jmat.2016.01.001

Khan AJ, Hanif M, Javed MS, Hussain S, Liu Z (2019) Synthesis, characterization and charge storage properties of C60-fullerene microparticles as a flexible negative electrode for supercapacitors. J Mater Sci Mater El 30:8568–8576. https://doi.org/10.1007/s10854-019-01177-4

Leiro JA, Heinonen MH, Laiho T, Batirev IG (2003) Core-level XPS spectra of fullerene, highly oriented pyrolitic graphite, and glassy carbon. J Electron Spectros Relat Phenomena 128:205–213. https://doi.org/10.1016/S0368-2048(02)00284-0

Lemine AS, Zagho MM, Altahtamouni TM, Bensalah N (2018) Graphene a promising electrode material for supercapacitors—A review. Int J Energ Res 42:4284–4300. https://doi.org/10.1002/er.4170

Lesiak B, Kövér L, Tóth J, Zemek J, Jiricek P, Kromka A, Rangam N (2018) C sp2/sp3 hybridisations in carbon nanomaterials—XPS and (X)AES study. Appl Surf Sci 452:223–231. https://doi.org/10.1016/j.apsusc.2018.04.269

Li Q, Horn M, Wang Y, MacLeod J, Motta N, Liu J (2019a) A review of supercapacitors based on graphene and redox-active organic materials. Materials 12:703. https://doi.org/10.3390/ma12050703

Li J, Shao Z, Ma Y, Qu Y (2019b) Graphene and their hybrid electrocatalysts for water splitting. ChemCatChem 21:801–825. https://doi.org/10.1002/cctc.201700175

Liu J, Cui L, Losic D (2013) Graphene and graphene oxide as new nanocarriers for drug delivery applications. J Acta Biomater 12:9243–9257. https://doi.org/10.1016/j.actbio.2013.08.016

Ma J, Guo Q, Gao HL, Qin X (2015) Synthesis of C_{60}/Graphene composite as electrode in supercapacitors. Fullerenes, Nanotubes, Carbon Nanostruct 23:477–482. https://doi.org/10.1080/1536383X.2013.865604

Mahmoudi T, Wang Y, Hahn Y-B (2018) Graphene and its derivatives for solar cells application. Nano Energy 47:51–65. https://doi.org/10.1016/j.nanoen.2018.02.047

Naebe M, Wang J, Amini A, Khayyam H, Hameed N, Li LH, Chen Y, Fox B (2015) Mechanical property and structure of covalent functionalised graphene/epoxy nanocomposites. Sci Rep 4:4375. https://doi.org/10.1038/srep04375

Najib S, Erdem E (2019) Current progress achieved in novel materials for supercapacitor electrodes: mini review. Nanoscale Adv 1:2817–2827. https://doi.org/10.1039/C9NA00345B

Onoe J, Nakao A, Takeuchi K (1997) XPS study of a photopolymerized C_{60} film. Phys Rev B 551:10051–10056. https://doi.org/10.1103/PhysRevB.55.10051

Peña-Bahamonde J, Nguyen HN, Fanourakis SK, Rodrigues DF (2018) Recent advances in graphene-based biosensor technology with applications in life sciences. J Nanobiotechnology 16:75. https://doi.org/10.1186/s12951-018-0400-z

Perreault F, Fonseca de Faria A, Elimelech M (2015) Environmental applications of graphene-based nanomaterials. Chem Soc Rev 44:5861–5896. https://doi.org/10.1039/C5CS00021A

Piotrowski P, Pawłowska J, Bilewicz R, Kaim A (2016) Selective and reversible self-assembly of C_{60} fullerene on a 9,10-bis(*S*-acetylthiomethyl)anthracene modified gold surface. RSC Advances 6:53101–53106. https://doi.org/10.1039/C6RA04806D

Poonam SK, Arora A, Tripathi SK (2019) Review of supercapacitors: materials and devices. J Energy Storage 21:801–825. https://doi.org/10.1016/j.est.2019.01.010

Pumera M (2011) Graphene in biosensing. Mater Today 14:308–315. https://doi.org/10.1016/S1369-7021(11)70160-2

Quintana M, Spyrou K, Grzelczak M, Browne WR, Rudolf P, Prato M (2010) Functionalization of Graphene via 1,3-Dipolar Cycloaddition. ACS Nano 4:3527. https://doi.org/10.1021/nn100883p

Rubino RS, Takeuchi ES (1999) The study of irreversible capacity in lithium-ion anodes prepared with thermally oxidized graphite. Journal of Power Sources: 81–82, 373–377. https://doi.org/10.1016/S0378-7753(99)00217-7

Shareena TPD, McShan D, Dasmahapatra AK, Tchounwou PB (2018) A review on graphene-based nanomaterials in biomedical applications and risks in environment and health. Nano-Micro Lett 10:53. https://doi.org/10.1007/s40820-018-0206-4

Sohmen E, Fink J, Kratschmer W (1992) Electron energy-loss spectroscopy studies on C_{60} and C_{70} fullerite. Z Phys B Condensed Matter 86:84–92. https://doi.org/10.1007/BF01323552

Su Y, Du J, Sun D, Liu C, Cheng H (2013) Reduced graphene oxide with a highly restored π-conjugated structure for inkjet printing and its use in all-carbon transistors. Nano Res 6:842–852. https://doi.org/10.1007/s12274-013-0362-2

Tran NE, Lambrakos SG, Lagowski JJ (2009) Analysis of capacitance characteristics of C_{60}, C_{70}, and La@C_{82}. J Mater Eng Perform 18:95–101. https://doi.org/10.1007/s11665-008-9267-8

Wang D-W, Li F, Wu Z-S, Ren W, Cheng H-M (2009) Electrochemical interfacial capacitance in multilayer graphene sheets: Dependence on number of stacking layers. Electrochem Commun 11:1729–1732. https://doi.org/10.1016/j.elecom.2009.06.034

Wang H, Yan X, Piao G (2017) A high-performance supercapacitor based on fullerene C60 whisker and polyaniline emeraldine base composite. Electrochim Acta 231:264–271. https://doi.org/10.1016/j.electacta.2017.02.057

Yulaev A, Cheng G, Walker ARH, Vlassiouk IV, Myers A, Leite MS, Kolmakov A (2016) Toward clean suspended CVD graphene. RSC Adv 6:83954–83962. https://doi.org/10.1039/C6RA17360H

Zhao S, Chen H, Qian Q, Zhang H, Yang Y, Hong W (2021) Non-covalent interaction-based molecular electronics with graphene electrodes. Nano Res. https://doi.org/10.1007/s12274-021-3687-2

Zuo Y, Gu J, Yang L, Qiao Z, Tan H, Zhang Y (2013) Synthesis and characterization of maleic anhydride esterified corn starch by the dry method. Int J Biol Macromolecules 62:241–247. https://doi.org/10.1016/j.ijbiomac.2013.08.032